Research Article

Umbreen Khattak, Samin Jan, Rehman Ullah, Tauheed ul Haq, Muhammad Nauman Khan, Majid Iqbal, Alevcan Kaplan*, Abdul Rehman*, Mohamed Farouk Elsadek, and Mohammad Ajmal Ali

Green synthesis and physical characterization of zinc oxide nanoparticles (ZnO NPs) derived from the methanol extract of *Euphorbia dracunculoides* Lam. (Euphorbiaceae) with enhanced biosafe applications

Abstract: *Euphorbia dracunculoides* Lam. possesses significant biological potential due to its rich bioactive compounds. To enhance this potential, zinc oxide nanoparticles (ZnO NPs) were synthesized using the methanolic extract of *E. dracunculoides*, exploiting ZnO NPs' superior physiochemical properties and bioavailability. The synthesis of ZnO NPs was confirmed through UV–Vis spectroscopy (with an absorption maximum at 368 nm), X-ray diffraction (crystalline nature), Fourier transform infrared spectroscopy (functional groups involved in Zn^{2+} reduction), scanning electron microscopy (rod-shaped and triangular morphologies, average size 79 nm), and EDX (presence of Zn and O). The ED-ZnO NPs exhibited dose-dependent cytotoxicity against U87 cells (IC_{50}: 229.51 µg·mL^{-1}) and anti-leishmanial activity against *Leishmania tropica* promastigotes (IC_{50}: 9.11 µg·mL^{-1}). Additionally, *in vivo* studies demonstrated significant antihyperlipidemic effects, with decreased cholesterol, triglyceride, and low-density lipoprotein levels, and increased high-density lipoprotein levels. ED-ZnO NPs also normalized alkaline phosphatase, alanine transaminase, aspartate transaminase, total bilirubin, creatinine, urea, and glucose levels compared to controls. Overall, ED-ZnO NPs effectively enhance the bioactive compounds' efficacy in treating various disorders.

Keywords: ED-ZnO NPs, GC–MS, *E. dracunculoides*, hepatoprotective potential, anticancer

* **Corresponding author: Alevcan Kaplan,** Department of Crop and Animal Production, Sason Vocational School, Batman University, Batman, 72060, Turkey, e-mail: kaplanalevcan@gmail.com
* **Corresponding author: Abdul Rehman,** Department of Physics, University of Strathclyde, Glasgow, G4 0NG, United Kingdom, e-mail: abdul.rehman@strath.ac.uk
Umbreen Khattak: Department of Botany, Islamia College, Peshawar, Pakistan, e-mail: fatimaktk60@gmail.com
Samin Jan: Department of Botany, Islamia College, Peshawar, Pakistan, e-mail: Samin@icp.edu.com
Rehman Ullah: Department of Botany, University of Peshawar, Peshawar, 25100, Pakistan, e-mail: rehmanbotany@uop.edu.pk
Tauheed ul Haq: Department of Botany, University of Peshawar, Peshawar, 25100, Pakistan, e-mail: tauheedbotany@gmail.com
Muhammad Nauman Khan: Department of Botany, Islamia College, Peshawar, Pakistan; University Public School, University of Peshawar, 25120, Peshawar, Pakistan, e-mail: nomiflora@uop.edu.pk
Majid Iqbal: Key Laboratory of Ecosystem Network Observation and Modeling, Institute of Geographic Sciences and Natural Resources Research, Chinese Academy of Sciences, 11A, Datun Road, Chaoyang District, Beijing, 100101, China; University of Chinese Academy of Sciences, (UCAS), Beijing, 100049, China, e-mail: miqbal@igsnrr.ac.cn
Mohamed Farouk Elsadek: Department of Biochemistry, College of Science, King Saud University, P.O. 2455, Riyadh, 11451, Saudi Arabia, e-mail: mfbadr@ksu.edu.sa
Mohammad Ajmal Ali: Department of Botany and Microbiology, College of Science, King Saud University, Riyadh, 11451, Saudi Arabia, e-mail: ajmalpdrc@gmail.com

1 Introduction

Nanotechnology is a rapidly growing field of science that offers great potential for improving human well-being in various areas. Nanoparticles (NPs) and nanomaterials continue to find new applications in scientific disciplines due to their remarkable flexibility and unique physicochemical properties. In contemporary times, metallic NPs have gained importance in various fields, such as biomedicine, electronics, catalysis, sensing, and biotechnology [1]. Their effectiveness is based on the fact that nanomaterials, due to their minuscule size of 1–100 nm and the resulting surface-to-volume ratio, have physicochemical properties that differ from those of their bulk counterparts [2]. The unique

structural properties of NPs, including their size, shape, and lattice configuration, give them extraordinary capabilities that can be used in various fields. These include textiles, electronics, pharmaceuticals, biomarkers, biosensors, and even biomedicine [3]. Among the remarkable NPs, those made of precious metals are mainly used due to their useful chemical, electrical, optical, mechanical, and magnetic properties, which are further enhanced by their large surface area and tiny particle size. This makes precious metal NPs indispensable in the fields of catalysis, photonics, and electronics [4].

Nature has endowed plants with a variety of secondary metabolites; these metabolites can serve as crucial redox mediators and stabilizers for NPs [5–8]. This symbiotic relationship between plants and NPs opens doors for novel applications, in which the unique chemical properties of plants synergistically interact with their characteristic attributes. Consequently, the convergence of nanotechnology and plant materials offers a promising avenue for innovative advances in various industries. The use of plant products/extracts for the synthesis of NPs offers a distinct advantage, due to their improved stability and simplified production processes compared to conventional methods.

These "green" approaches are not only in line with environmental sustainability but also offer cost efficiency, simplicity, and safety by eliminating the use of toxic substances [9,10]. This move towards green synthesis utilizes the inherent properties of plant-derived compounds, which help to enhance the stability and functionality of the resulting NPs. Metal oxide NPs show enormous potential for various biomedical applications. They have been discovered for their role in cell imaging technologies, antibacterial treatments, bio-sensing systems, and even as agents for anti-cancer drugs and gene transfer [11]. The unique attributes of metal oxide NPs, combined with their environmentally friendly plant-based synthesis, open up a wide range of possibilities in biomedical research. This convergence of environmentally friendly synthesis methods and the versatile applications of metal oxide NPs represents an exciting avenue for advancing medical technologies and finding cures for life-threatening ailments.

Zinc (Zn) is an essential micronutrient, that plays a role in more than 300 enzyme structures and is involved in a number of vital bioprocesses. Its involvement in signaling pathways extends to hepatic glycogenesis and improves glucose uptake. In addition, Zn plays a pivotal role in insulin-related mechanisms, involving generation, secretion, and signaling, all of which together influence the metabolic function of insulin itself [12]. In the field of biological applications, zinc oxide nanoparticles (ZnO NPs) have proven to be a promising option. They are characterized by environmental compatibility, simple production methods, non-toxicity, biosafety, and biocompatibility. The recognition of ZnO, including its nanoparticulate form, as generally recognized as safe by the US Food and Drug Administration underscores its safety profile [13]. Due to these favorable properties, ZnO NPs are suitable candidates for a wide range of applications ranging from cosmetics and drug delivery systems to anticancer agents, antidiabetics, cell imaging tools, antimicrobials, and biosensors. The different physicochemical properties of ZnO NPs highlight their divergence functions [14].

Interestingly, human cells remain unaffected by ZnO NPs, while these NPs exhibit adverse effects on bacteria and other microorganisms. Importantly, Zn ions do not interfere with DNA in human cells, and these NPs are well tolerated by human cell systems. Moreover, ZnO is effective in various catalytic reaction processes due to its strong catalytic activity and large surface area [15]. Likewise, the extensive applications of ZnO NPs span the fields of biological sensing, gene transfer, biological labeling, drug delivery, and nanomedicine, imparting transformative potential for various biological contexts. This convergence of the exceptional properties of ZnO NPs and their diverse applications underscores their importance for progress in both biological research and practical applications [16].

Medicinal plants play a promising role in the modulation of several human disorders. Many civilizations and cultures such as Ayurvedic, Chinese, and Unani culture have used these plants extensively to treat their health problems. Plant-derived chemicals (phyto-chemicals) are important sources of clinical agents that have sedative, antidepressant, antioxidant, antispasmodic, anti-inflammatory, analgesic, cardio-protective, etc., effects, *Euphorbia dracunculoides* belongs to the Euphorbiaceae plant family. In the aerial parts of this plant, researchers have identified and isolated 19 structurally distinct diterpenoids and other compounds, as highlighted by Wang et al. [17] and other researchers. These compounds such as terpenoids, coumarins, flavonoids, tannins, phenols, alkaloids, and betacyanin have been detected in various studies of *E. dracunculoides* using advanced analytical techniques such as high-performance liquid chromatography and nuclear magnetic resonance. This plant is of great medicinal importance as it contains a variety lot of phytochemicals. Traditional applications include the use of decoctions from the entire plant to treat cattle to effectively control mice infestations. The fruit of *E. dracunculoides* is known for its purported ability to remove warts from the skin. Furthermore, the leaf paste is used in combination with black pepper and ghee to treat snake bites, while the leaf powder is used to treat epilepsy [18]. We are more at risk from reactive oxygen species

(ROS) and reactive nitrogen species as they are generated during the normal metabolic process in the human body and these free radicals cause numerous life-threatening disorders. Phytochemicals play a unique role in preventing the dangerous effects of free radicals [19]. Polyphenols are excellent free radical scavengers and inhibitors of lipid peroxidation. Terpenoids and steroids are useful metabolites in various metabolic disorders. These properties make their role crucial from a therapeutic and pharmacological point of view. Besides these diverse biological applications of the phyto-chemicals present in the plant, there are also some limitations such as minimal solubility, poor stability, and large molecular size that hinder their bioavailability. Furthermore, to the best of our knowledge, the traditional applications of this plant are numerous, but the biological applications of the phyto-metabolites of this plant with NPs are undiscovered. So this work was designed with the aim of further improving the bioavailability of these phytochemicals present in *E. dracunculoides* we utilize the methanol extract of the plant as a reducing agent for the synthesis of ZnO NPs and then characterize and evaluate the biological potential *in vivo* and *in vitro*.

2 Materials and methods

2.1 Preparation of the *E. dracunculoides* whole plant methanolic fraction

The specimens of *E. dracunculoides* were precisely collected from the southern districts of Khyber Pakhtunkhwa and then thoroughly washed and carefully soaked. The plant material was then dried in the shade. A comprehensive herbarium sheet with all relevant information was prepared, and the specimens were officially submitted to the Department of Botany University of Peshawar for documentation. A stepwise process was followed to prepare the plant material for analysis. The dried plant material was ground into a fine powder using an electric grinder. This pulverized material was then subjected to extraction by soaking in 80% ethanol at a temperature of 37°C for 72 h. During this period, the extraction process was facilitated by manual shaking. The resulting mixture was then filtered using Whatman filter paper No. 1. The collected filtrate was concentrated using a rotary evaporator and maintaining a heating bath at 40°C, forming a dark green semi-solid greenish semisolid material. This concentrated extract was then suspended in distilled water and methanol.

A gas chromatography–mass spectrometry (GC–MS) instrument (model QP2010, manufactured by SHIMADZU)

was used for GC–MS analysis of the methanol fraction of *E. dracunculoides*. Using a Db 30.0 column with a film diameter and thickness of 0.25 μm, the chromatogram was generated. The GC–MS-QP2010 device was equipped with an electronic pressure control, which enabled automatic sample injection. The oven temperature was programmed to increase gradually an incremental increase from 70°C to 200°C to 280°C over a period of 5 min. The carrier gas was highly purified helium (He) at a flow rate of 0.8 mL·min^{-1}. An ionization voltage of 70 eV was applied. The compounds in the methanol fraction were identified by matching their mass spectra with the library maintained by the National Institute of Standards and Technology and Wiley, which enabled the characterization and understanding of the chemical constituents present in the methanol fraction of *E. dracunculoides*.

2.2 Green synthesis of ZnO NPs

The green synthesis process for the synthesis of ED-ZnO NPs was carried out using chemicals and equipment, i.e. zinc sulfate ($ZnSO_4 \cdot 7H_2O$), magnetic stirrer, sodium hydroxide (NaOH), deionized Milli-Q water, beakers, balance, water bath, Petri dish, and oven. Initially, 0.2 g of the methanolic fraction of *E. dracunculoides* was dissolved in 100 mL of water. Concurrently, a 1 mM Zn sulfate solution (0.00278 g/100 mL) was prepared in water. This solution was stirred continuously for about 1 h using a magnetic stirrer. In the next step, the gradual addition of the plant extract solution was added to the Zn sulfate solution in a 1:1 ratio. Subsequently, 0.02 M NaOH was carefully added dropwise to achieve a pH value of 12. Constant stirring was carried out throughout the process. The reaction mixture containing the plant extract, Zn sulfate, and NaOH, was incubated at a temperature of 60°C for 2 h. This incubation was carried out in the dark to prevent possible photocatalytic reactions. As the process progressed, a white-yellow colored precipitate formed *in situ*, indicating the successful formation of ED-ZnO NPs. After completion of the reaction, the resulting mixture was centrifuged. The precipitate was then washed successively with double distilled water and ethanol, both kept at a temperature of 60°C. The washed precipitate was then dried overnight in an oven. The final ZnO NP product, now in the form of a white-yellow colored substance, was stored in an amber-colored sample bottle for later use. This synthesis method offers an environmentally friendly approach to the production of ED-ZnO NPs, which can be used in various fields due to their unique properties resulting from the formation of NPs [20].

2.3 Physical characterization of green-synthesized ZnO NPs

Comprehensive physical characterization endeavors, including UV–visible spectroscopy, X-ray diffraction (XRD), Fourier transform infrared (FTIR) analysis, scanning electron microscopy (SEM), transmission electron microscopy (TEM), and energy-dispersive X-ray spectroscopy, collectively contribute to a thorough understanding of the synthesized ZnO NPs. A UV-1602 double beam UV–visible spectrophotometer "BMS (Biotechnology Medical Services)" with a resolution of 1 nm and a wavelength range of 200 to 500 nm was used to measure the UV spectra of the synthesized NPs. An X-ray diffractometer (JEOL JDX 3532) was used to examine the crystalline pattern of the biosynthesized ED-ZnO NP*s*. The analysis was performed with a nickel monochromator to filter the wavelengths. The tube voltage was set to 40 kV, the tube current was 30 mA, and Cu-K radiation was used. Furthermore, the functional groups in the plant extract and in the synthesized ED-ZnO NP*s* were identified by FTIR spectroscopy ("PerkinElmer spectrometer FTIR SPECTRUM ONE"). This analysis was performed with a resolution of $4 \, \text{cm}^{-1}$, covering the range from 4,000 to $0 \, \text{cm}^{-1}$. The morphology of the NPs was analyzed by SEM using the JSM-5910-JEOL-JAPAN model. TEM using the Philips Tacna G2 FEI F12 at Brown University, Rhode Island, USA, was used to further investigate the morphology and size of the ED-ZnO NP*s*. The qualitative and quantitative determination of ED-ZnO NP*s* was carried out using an energy-dispersive X-ray spectrometer INCA 200 from Oxford Instrument, UK. This analysis was carried out in conjunction with an SEM (JSM-5910). The Malvern Zeta Sizer was used for dynamic light scattering (DLS) analysis and zeta potential distribution of ED-ZnO NPs. These characterization techniques provide insights into their structural, morphological, and compositional properties and reveal the special qualities of the NPs produced by green synthesis.

2.4 Cytotoxicity assay against U87 malignant glioma tumor cells

In the current study, a cytotoxicity assay against U87 malignant glioma tumor cells was performed to determine the cytotoxic potential of ED-ZnO NP*s* following Rezadoost et al. [21]. The U87 cells, which were obtained from the American Type Culture Collection in Rockville, MD, USA, were cultured in 96-well plates for the assay. After an incubation period of 24 h, the cells were seeded in 96-well plates. To assess the cytotoxic potential of the ED-ZnO NP*s*, the cells were treated in triplicate with NPs at varying concentrations ranging from 500 to 6.25 μM. The plates were then incubated for a further 24 h after treatment with following the application of the NPs. The next day, the cells were observed under a phase contrast microscope, and representative images were taken. For further analysis of the cells, they were rinsed, fixed with formalin, and stained with crystal violet. The absorbance of the cells was then measured at a wavelength of 630 nm using a 96-well plate reader (BioTek). The percentage inhibition of cell viability was calculated using the following formula:

$$\%\text{inhibition of cell viability} = \frac{\text{control} - \text{treatment}}{\text{control}} \times 100.$$

This indicator provides information on the extent of the cytotoxic effects induced by the treatment. Finally, the IC_{50} value, which indicates the concentration at which the NP treatment leads to a 50% decrease in cell viability, was determined using GraphPad Prism 8 software.

2.5 Anti-leishmanial effects against promastigote forms

The antileishmanial effect of ZnO NPs, mediated by *E. dracunculoides,* on promastigote forms of *Leishmania tropica* was investigated using a colorimetric cell viability assay, specifically the MTT assay. This procedure followed a methodology previously described in studies by Mahmoudvand et al. [22] and Mirzaie et al. [23]. In this assay, a 96-well microtiter plate was used as an experimental platform. Initially, each well was filled with 100 μL of promastigotes in the logarithmic growth phase (10^6 cells·mL^{-1}). Subsequently, 100 μL of different concentrations (5, 10, 15, and 20 μg·mL^{-1}) of the test samples, consisting of ZnO NPs, mediated by *E. dracunculoides*, were added to the respective wells. The plate was then incubated at 25°C for 72 h. Promastigotes without the NPs served as a control group and were provided with RPMI 1640 medium supplemented with 15% fasting blood sugar (FBS). Additionally, three wells containing only 100 μL of culture medium were designated as blank wells to account for any background effects. After the 72 h incubation period, 20 μL of MTT solution (5 mg·mL^{-1}) was added to each well, and the plate was kept in a dark room at 25°C for 4 h. After this incubation, the cells were centrifuged at 3,000 rpm for 10 min, resulting in cell pellets. These pellets were treated with 100 μL of dimethyl sulfoxide and incubated again. To generate a purple color indicative of formazan crystals, cold isopropanol was used as a solvent. Finally, an ELISA reader (BioTek-ELX800) was used to measure the absorbance in each well at a wavelength of 630 nm. The percentage inhibition of promastigote viability was calculated using the following formula:

$$\%\text{inhibition} = 1 - \frac{\text{absorbance of the sample}}{\text{absorbance of control}} \times 100.$$

2.6 Antihyperlipidemic and hepatoprotective activity

The research focused on investigating the anti-hyperlipidemic (cholesterol-lowering) effect of ZnO NPs in a controlled experiment with 36 healthy American albino mice. These mice, weighing between 20 and 30 g, were bred in the animal facility of the Veterinary Research Institute. During the 3-week duration of the study, the mice were housed in plastic cages and provided with regular laboratory food and water. The study comprised six different groups, each consisting of six mice. Group 1 received normal saline along with standard food and served as a control group. Group 2 was given a high-fat diet (positive control). Group 3 received a high-fat diet together with the standard drug rosuvastatin. In group 4, the mice received a high-fat diet together with ED-ZnO NPs at a dose of 100 mg·kg^{-1} body weight. Group 5 received the same high-fat diet together with ED-ZnO NPs at a dosage of 200 mg·kg^{-1} body weight. Group 6 was given a high-fat diet in combination with ED-ZnO NPs. All groups, except the positive control, received a mixture of edible coconut oil and vanaspati ghee in a volume/volume ratio of 3:2 according to a procedure developed by Khan et al. [24]. This mixture was administered orally to the mice daily for 1 week at a dose of 0.2 mL/30 g body weight in addition to their regular diet. The mice in the positive control group were euthanized on the seventh day. Blood samples were taken from the orbital region of the mice and filled into heparin tubes. The remaining groups were euthanized 14 days after receiving the respective treatment. Blood samples were centrifuged at 10,000 rpm to obtain plasma, which was then stored at 20°C for subsequent analysis of lipid profiles, including total cholesterol (TC), triglycerides, low-density lipoprotein (LDL), and high density lipoprotein (HDL). Liver parameters such as alanine transaminase (ALT), aspartate transaminase (AST), alkaline phosphatase (ALP), and total bilirubin, as well as renal parameters such as urea and creatinine were also measured. Fasting blood glucose levels were also determined. The analyses were conducted at the Doctor Diagnostic Lab in Hayatabad Hospital Complex, Peshawar. The collected data were subjected to statistical analysis using one-way analysis of variance followed by Dunnett's test using GraphPad Prism 8 software. The results are expressed as mean ± standard error of the mean.

3 Results

3.1 Biosynthesis of ZnO NPs using *E. dracunculoides* methanolic extract

ZnO NPs were synthesized by a process using a methanolic extract of *E. dracunculoides*. The process was initiated with the stepwise addition of the methanolic fraction of the
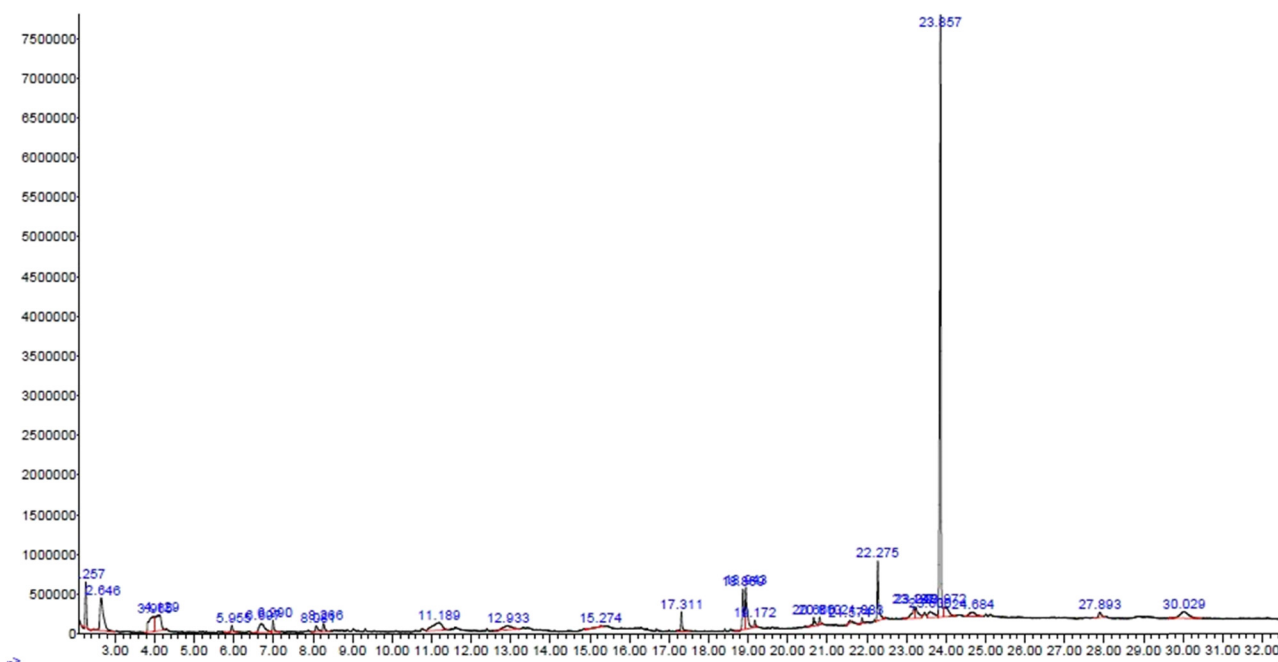

Figure 1: GC–MS chromatogram of methanolic extract of *E. dracunculoides* for RT values ranging from 0 to 32 min.

plant extract to a Zn sulfate solution in a 1:1 ratio. NaOH was then added dropwise to the mixture. This sequential addition resulted in the formation of a white-yellow colored precipitate, which served as a visual indicator for the successful formation of ZnO NPs (ED-ZnO NPs) at the end of the process. Analysis of the methanolic extract of *E. dracunculoides* by GC–MS revealed the presence of 25 known phytochemical compounds (Figure 1). Among these compounds, the compound 1,4-benzenedicarboxylic acid, bis(2-ethylhexyl) ester exhibited the highest peak area, with 41.54% of the total. Other compounds identified are carbonic acid, dimethyl ester, oleic acid, erucic acid, glycerin, ᴅ-glucohexodialdose, and propane, 2-methyl-2-(1-methylethoxy), with peak area percentages of 6.41%, 4.45%, 4.41%, 3.94%, 3.94%, and 2.96%, respectively (Table 1).

3.2 Characterization of ZnO NP-mediated *E. dracunculoides* extract

3.2.1 UV–visible spectroscopy of ED-ZnO NPs

The presence of was confirmed by UV-Vis spectroscopy. The UV spectrum of the colloidal solution exhibited a clear absorption peak at 368 nm (Figure 2). The use of bioactive plant compounds such as terpenoids, alkaloids, flavonoids, and tannins, in the methanolic extract of *E. dracunculoides* reduces Zn^{2+} ions to ZnO to form stable ED-ZnO NPs. This green synthesis approach also ensures that the reduction process is environmentally friendly and sustainable. The observed absorption peak at 368 nm in the UV spectrum is consistent with the characteristic plasmon resonance of Zn NPs. The phytometabolites present in the leaf extract of *E. dracunculoides* play a dual role: they act as reducing agents that facilitate the conversion of Zn^{2+} ions into ZnO NPs, and as stabilizers that surround and cover the formed NPs, preventing agglomeration. The results of this study are in agreement with previous research by Kumar et al. [25] who also found plasmon peaks in the range of 365 to 375 nm.
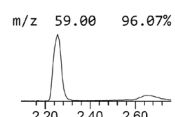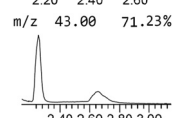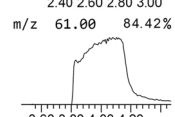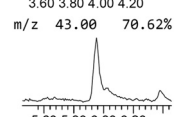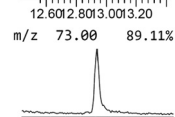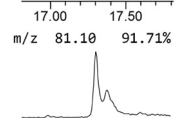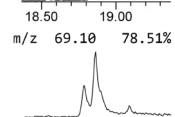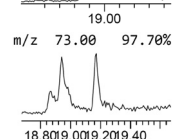
3.2.2 XRD analysis of ED-ZnO NPs
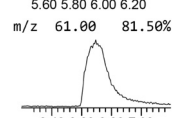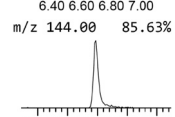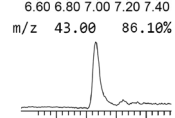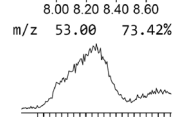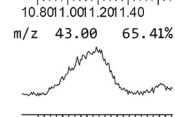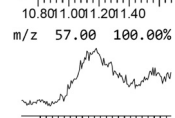
The crystalline structure of ED-ZnO NPs was elucidated by XRD analysis. The XRD spectrum exhibited distinct peaks corresponding to 2θ angles of 31.75° (100), 34.35° (002), 36.2° (101), 47.5° (102), 56.6° (110), 62.9° (103), 68.05° (112), and 69.2° (201) Bragg's reflections (Figure 3). These peaks are indicative of the crystalline nature of the synthesized nanocrystalline ED-ZnO NPs. The XRD pattern of the sample agrees

very well with the reference data from the International Center for Diffraction Data database (JCPDS-36-1451), confirming the purity of the synthesized iron oxide NPs. The observed XRD peaks demonstrate the crystalline integrity of the ED-ZnO NPs and confirm their formation and agreement with the established crystallographic data. The presence of additional peaks indicates that biomolecules from the plant extract were absorbed on the surface of the ED-ZnO NPs, possibly contributing to their stabilization. The crystalline size of the ED-ZnO NPs was calculated using the full width at half maximum (FWHM) (β = 0.0029 radians or 0.167°) of the 101 plane of the XRD spectrum at 2θ of 36° and determined to be approximately 50 nm using the Debye–Scherrer equation, emphasizing their nanoscale dimensions. The lattice constant for hexagonal wurtzite crystals of ZnO NPs was also calculated using the equation ($n\lambda = 2d_{hkl} \sin\theta$), and the base of the hexagonal unit cell was found to be a = 3.23 Å whereas the height was found to be c = 5.18 Å. The strain of ED-ZnO NPs was calculated from the difference between the lattice competitor of ZnO NPs and the counterpart ZnO. The strain of the a-axis (ϵ_a) was estimated to be 0.9%, while the strain of the c-axis (c_a) was estimated to be 0.4%. In summary, this description describes the XRD analysis performed to determine the crystalline nature of the ZnO NPs with reference to the established Bragg reflexes.
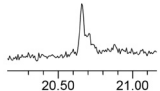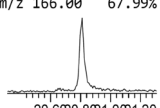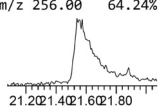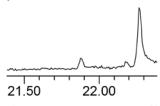
3.2.3 FTIR spectroscopy
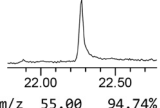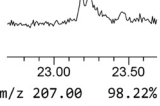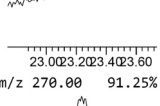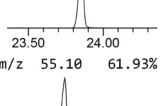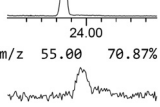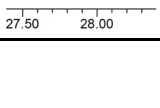
In the current study, FTIR was used to analyze the distinct bands of ED-ZnO NPs and untreated plant extract (depicted in Figure 4a and b). Specific vibrational patterns were identified in the FTIR spectrum of the plant extract: a peak at 3,307 cm^{-1} denoting O–H bonding of phenol and alcohol, another at 2,931 cm^{-1} indicating C–H bending in alkanes, 1,619 cm^{-1} associated with C꞊C bending in conjugated alkenes, which also corresponds to amide I of polypeptides, 1,408 cm^{-1} for the S꞊O stretching in sulfonyl chloride, 1,258 cm^{-1} for the C–O bending in aromatic esters, 1,040 cm^{-1} reflecting C–N bending in amines, 987 cm^{-1} indicating C꞊C bending in alkenes, 923 cm^{-1} for the C꞊C bending in alkenes, and 776 cm^{-1} for the C–H bending. Conversely, the FTIR spectrum of ED-ZnO NPs showed prominent vibrations at 3,348, 1504, 1388, 1095, 958, and 598 cm^{-1}, which were associated with O–H stretching (alcohol/phenol), N–O bending (nitro compounds), C–H stretching (aldehyde), C–O and C–N bending (primary alcohol, amine), C꞊C bending (alkene group), and Zn–O bending. Nota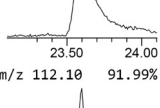bly, the shift of the C–H and C꞊C stretches in the IR spectrum of ED-ZnO NPs indicates that the phytochemicals are bound to the surface of the synthesized ED-ZnO NPs. The presence of

Table 1: GC–MS profile of the crude methanol extract of *E. dracunculoides*

S. no.	RT	Compound	Peak % area	Mass spectra	M. mass (g·mol^{-1})
1	2.257	Propane,2-methyl-2-(1-methylethoxy)-	2.96	m/z 59.00 96.07%	116.2
2	2.647	Carbonic acid, dimethyl ester	6.41	m/z 43.00 71.23%	90.08
3	3.963	Glycerin	3.94	m/z 61.00 84.42%	92.09
4	5.952	4(1*H*)-Pyrimidinone, 2,6-diamino-	0.56	m/z 43.00 70.62%	126.12
5	6.697	Diglycerol	2.63	m/z 61.00 81.50%	166.17
6	6.990	4*H*-Pyran-4-one, 2,3-dihydro-3,5-dihydroxy-6-methyl	0.95	m/z 144.00 85.63%	144.12
7	8.081	5-Hydroxymethylfurfural	0.82	m/z 43.00 86.10%	126.11
8	8.266	1,2,3-Propanetriol, 1-acetate	0.83	m/z 53.00 73.42%	134.13
9	11.189	D-Glucohexodialdose	3.94	m/z 43.00 65.41%	178.14
10	12.933	alpha,beta-Gluco-octonic acid lactone	1.90	m/z 57.00 100.00%	238.1920
11	17.311	*n*-Hexadecanoic acid	1.48	m/z 73.00 89.11%	256.42
12	18.869	(9*E*,11*E*)-Octadecadienoic acid	2.91	m/z 81.10 91.71%	280.4
13	18.943	Oleic acid	4.45	m/z 69.10 78.51%	282.5
14	19.172	Octadecanoic acid	0.43	m/z 73.00 97.70%	284.5

(Continued)

Table 1: *Continued*

S. no.	RT	Compound	Peak % area	Mass spectra	M. mass (g·mol^{-1})
15	20.66	*cis*-11-Eicosenoic acid	0.88	m/z 83.10 77.52% 20.50 21.00	310.5
16	20.81	2-Propen-1-one,1-(2,6-dihydroxy-4-methoxyphenyl)-3-phenyl-, (*E*)-	0.47	m/z 166.00 67.99% 20.60 20.80 21.00 21.20	270.28
17	21.574	4*H*-1-Benzopyran-4-one, 2,3-dihydro-5,7-dihydroxy-2-phenyl-, (*S*)-	0.24	m/z 256.00 64.24% 21.20 21.40 21.60 21.80	256.25
18	21.883	1-Benzazirene-1-carboxylic acid, 2,2,5a-trimethyl-1a-[3-oxo-1-butenyl] perhydro-, methyl ester	0.22	m/z 57.00 95.33% 21.50 22.00	265.35
19	22.275	Erucic acid	4.41	m/z 69.10 84.04% 22.00 22.50	338.6
20	23.187	1*S*,4*aS*,4*bS*,7*S*,8*aS*,10*aS*)-7-Isopropyl-1,4*a*-dimethyltetradecahydrophenanthrene	1.67	m/z 55.00 94.74% 23.00 23.50	262.5
21	3.24	7-Pentadecyne	1.80	m/z 207.00 98.22% 23.00 23.20 23.40 23.60	208.38
22	23.6	3,5-Androstandien-17-one	1.81	m/z 270.00 91.25% 23.50 24.00	270.4
23	23.857	1,4-Benzenedicarboxylic acid, bis(2-ethylhexyl) ester	41.54	m/z 112.10 91.99% 23.50 24.00	390.6
24	23.972	2-(Acetoxymethyl)-3-(methoxycarbonyl)biphenylene	2.51	m/z 55.10 61.93% 24.00	282.29
25	27.893	1-(3-Chlorophenyl)-3-methyl-1*H*-pyrazol-5-amine	0.64	m/z 55.00 70.87% 27.50 28.00	207.66

a peak at 598 cm^{-1} within the IR bands of ED-ZnO NPs confirmed the synthesis of ZnO bonds, as peaks falling in the 500–900 cm^{-1} range typically indicate metal oxygen groups, as previous studies by Rahaiee et al. have shown [26]. A variety of phytometabolites have been documented to play a crucial role in the reduction of ZnSO$_4$ to ZnO NPs.

3.2.4 SEM analysis

In the study, SEM was used to assess the surface morphology and dimensions of ZnO NPs synthesized by a green process. SEM analysis revealed a diverse spectrum of NP sizes, with an average size of 79 nm, as illustrated in Figure 5. The
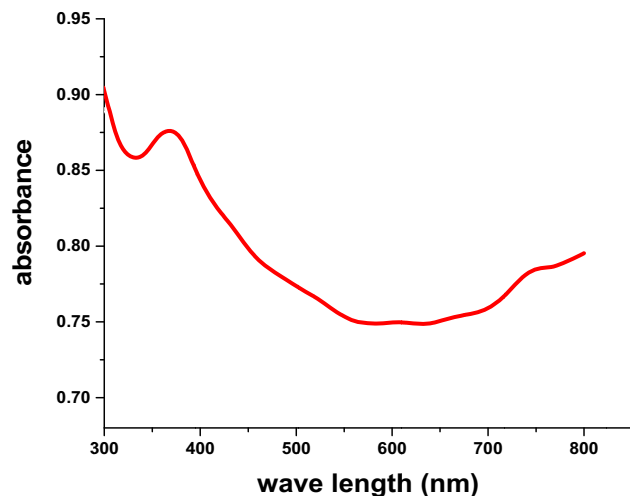
Figure 2: Ultraviolet–visible absorption spectra of ED-mediated ZnO NPs.

Figure 3: X-ray diffractogram of ED-ZnO NPs showing crystalline nature.

topographical characteristics of these NPs exhibited a remarkable variety of shapes, which included rod-shaped, spherical, and triangular shapes, and were often arranged in clusters. The surfaces of the NPs exhibited a rough texture. These morphological characteristics are consistent with previous studies reporting analogous shapes and textures [27].

3.2.5 TEM analysis

The structure and morphology of the NPs were confirmed using TEM. The TEM analysis involved a detailed examination of micrographs, which revealed that the NPs ranged in size from 18 to 118 nm with an average particle size of 66.93 nm (Figure 6). The Gaussian fit model of the size distribution gave an R^2 value of 0.973 and a chi-squared value
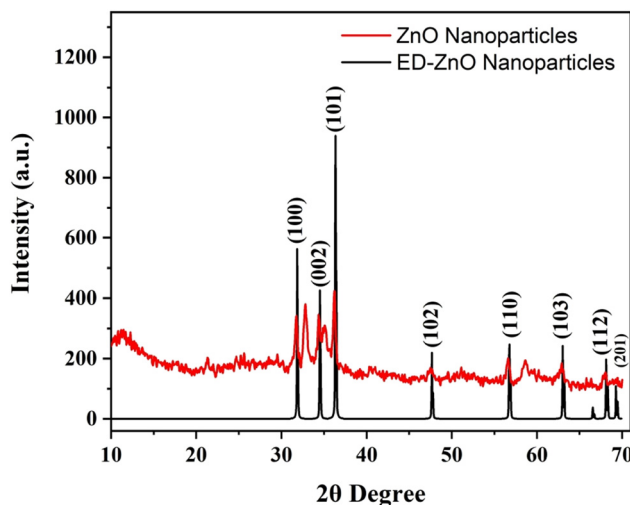
of 0.536. The FWHM of the Gaussian fit was found to be 35.95 nm. In terms of shape, the predominant morphology observed was spherical, although occasional cubic shapes were also noted (Figure 6). These results are in agreement with previous studies by Datta et al. [28] and Singh et al. [29], as shown by a number of published studies. The convergence of the results of across these different studies emphasizes the strength and reproducibility of the observed properties of the NPs.

3.2.6 Energy dispersive X-ray spectroscopy (EDS) analysis

EDS was used to analyze the elemental composition of the ED-ZnO NPs. The EDS analysis confirmed the presence of the elements Zn and oxygen (O), with weight percentages
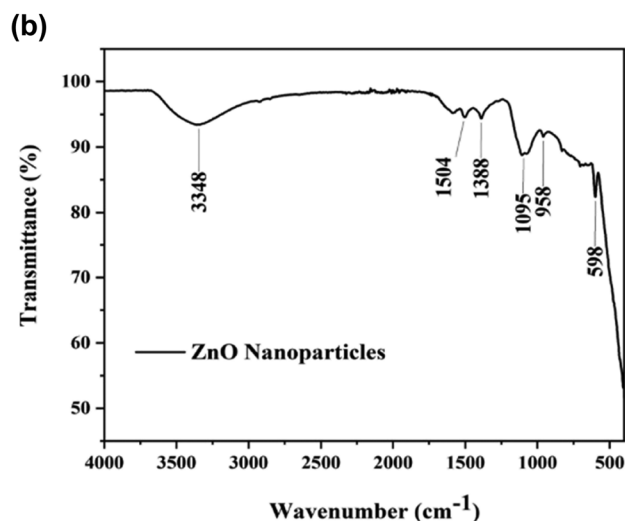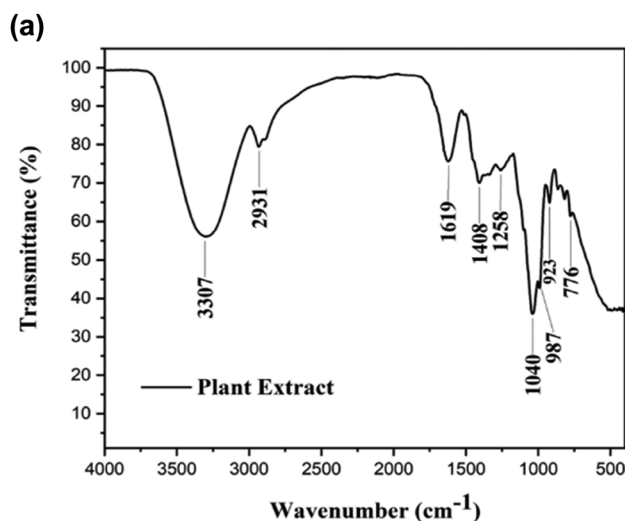

Figure 4: IR spectroscopy of *E. dracunculoides* extract and ED-ZnO NPs showing diverse functional groups stabilizing the NPs.
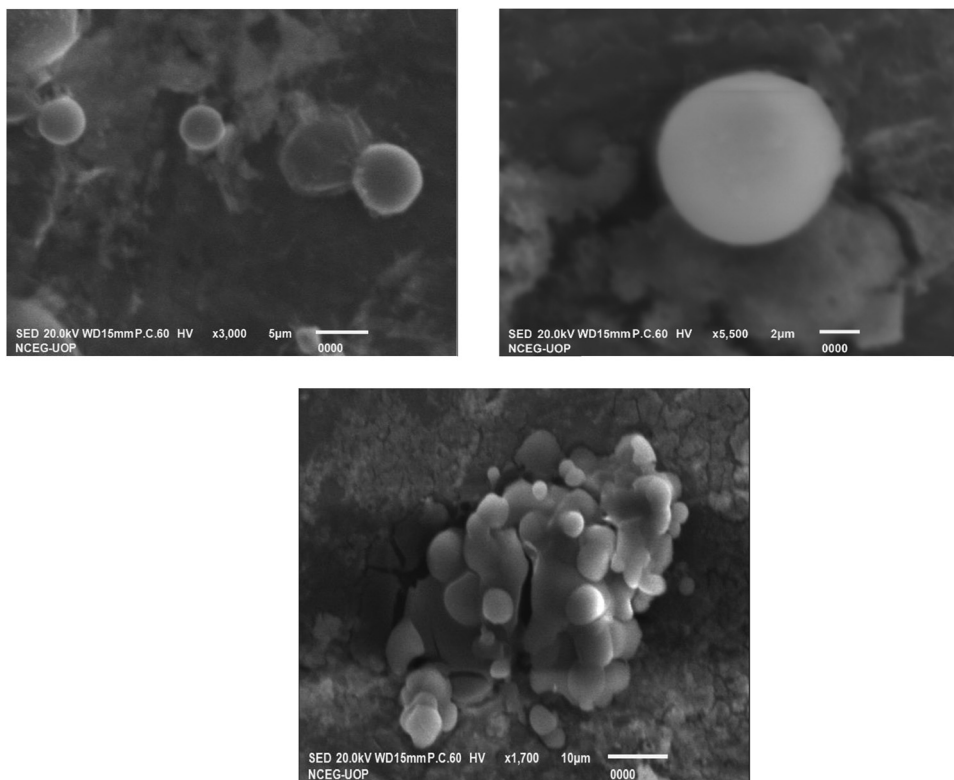
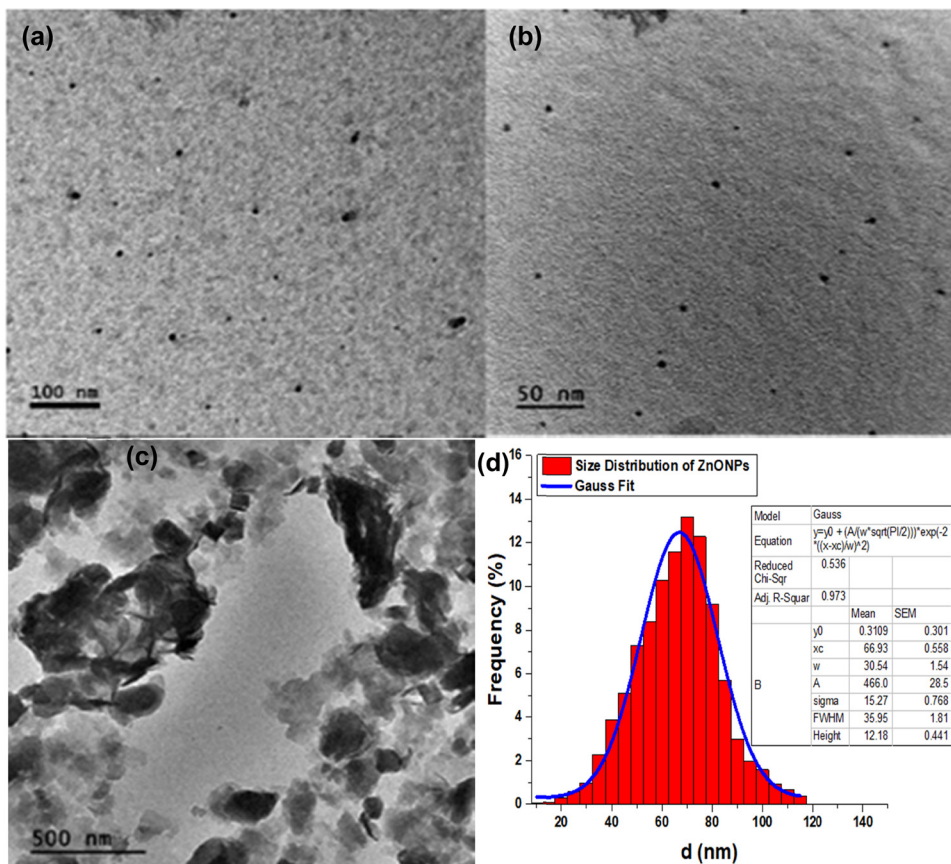**Figure 5:** SEM analysis of *E. dracunculoides* ZnO NPs.

Figure 6: TEM images of *E. dracunculoides* functionalized zinc nanoparticles (a–c) and their size distribution with Gaussian fit (d).
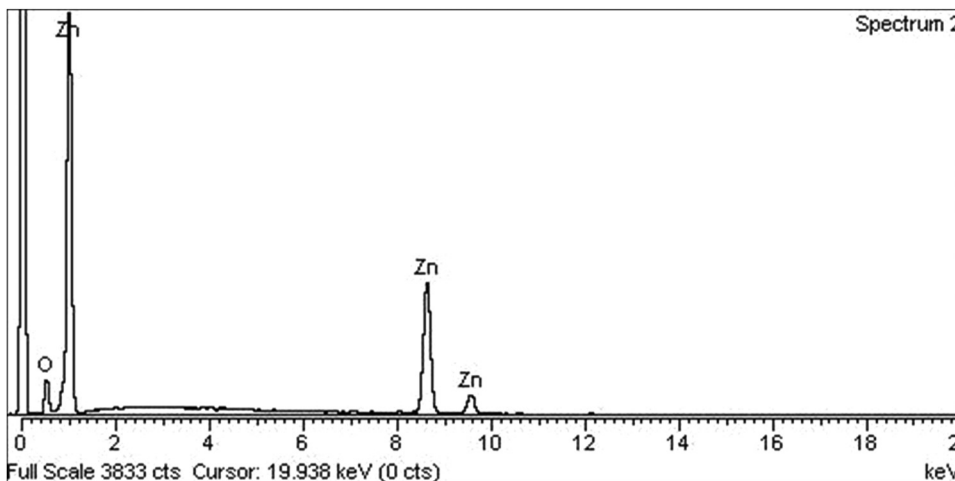
Figure 7: EDX of methanolic extract-mediated zinc oxide nanoparticles of *E. dracunculoides*.

of 71% and 29%, respectively. Remarkable peaks corresponding to Zn were observed at energy levels of 1 and 8.6 keV, and slightly above 9.6 keV. In the case of oxygen, a strong singular peak was observed at 0.5 keV (depicted in Figure 7). These EDS results are in agreement with the results of earlier studies by Vinayagam et al. [30] and Jayappa et al. [25], as shown in their published research papers. This agreement between the results of different studies emphasizes the agreement and validation of the elemental composition of the NPs determined by EDS analysis.

3.2.7 DLS spectroscopy and zeta potential

DLS analysis of the ED-functionalized ZnO NPs shows an average hydrodynamic particle diameter of 56.84 nm and a PDI of 0.402, indicating a moderate size variation and a bimodal distribution with both small and large particles (Figure 8). The zeta potential is −18.4 mV, indicating a moderately negative surface charge and relatively low electrostatic stability, possibly due to the capping of the phytometabolites associated with the ED extract. This charge may cause some repulsion between particles but may still

Figure 8: DLS spectrogram of ED-ZnO NPs, showing the mean hydrodynamic particle size of 56.84 nm with moderate polydispersity index and a zeta potential of −18.4 mV.

Table 2: Dose-dependent responses of ED-ZnO NPs on the growth of U87 cancer cells, with an IC_{50} value

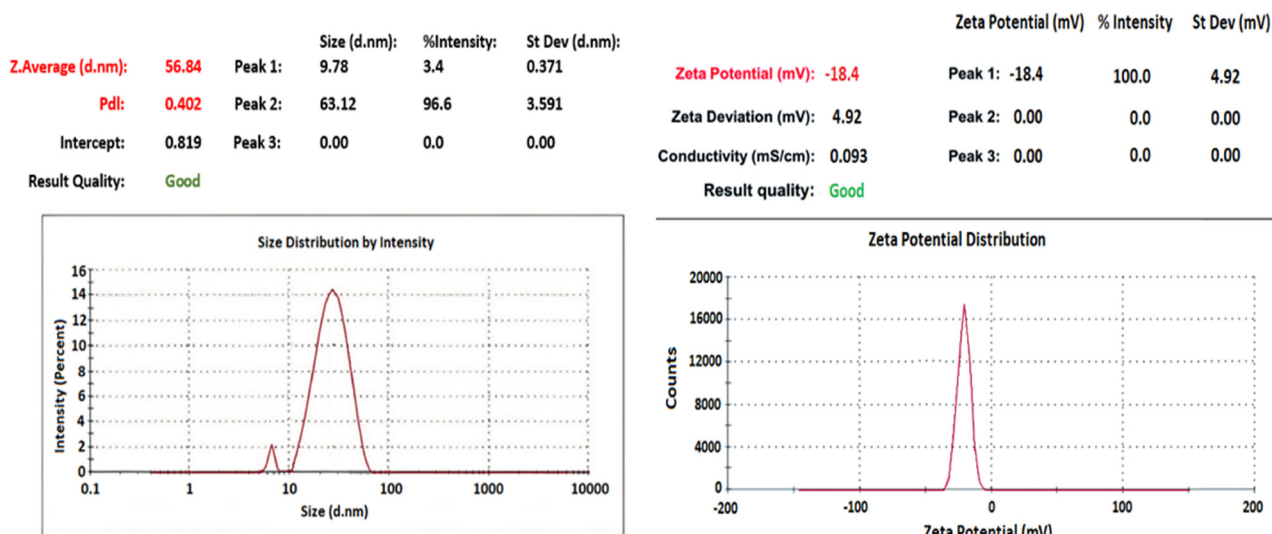| Concentration ($\mu g \cdot mL^{-1}$)	Zinc oxide nanoparticles		EC_{50} ($\mu g \cdot mL^{-1}$)	EC_{70} ($\mu g \cdot mL^{-1}$)	EC_{90} ($\mu g \cdot mL^{-1}$)	Intercept	Slope	F	R^2	p
	Mean absorbance	Percent inhibition								
500	0.101	72.25	239.30	385.28	513.27	17.216	0.137	20.32	0.734	0.004
250	0.114	68.68								
125	0.18	50.54								
62.5	0.242	33.51								
31.25	0.282	22.52								
15.62	0.314	13.73								
7.81	0.319	12.36								
Negative control	0.364	0								

be susceptible to changes in the medium. Additionally, the conductivity of 0.093 ms·cm^{-1} reflects the ionic strength of the suspension, which may affect both the zeta potential and the overall stability of the NPs.

3.2.8 *In vitro* cytotoxicity (antitumor activity)

In the current *in vitro* cytotoxicity assessment, the application of ZnO NPs (ED-ZnO NPs) resulted in a significant reduction in the viability of human glioma cell U87. The presence of ED-ZnO NPs led to a remarkable reduction in the growth of U87 brain cells, resulting in percentage mortality values of 72.25%, 68.68%, 50.54%, 33.51%, 22.52%, 13.73%, and 12.36% at different doses: 500, 250, 125, 62.5,

31.25, 15.62, and 7.81 $\mu g \cdot mL^{-1}$, respectively (Table 2). This dose-dependent response illustrated that ED-ZnO NPs had a significant inhibitory effect on the growth of U87 cancer cells, with an IC_{50} value of 239.30 $\mu g \cdot mL^{-1}$ after a 24 h exposure period (Figure 9).

3.2.9 Antileishmanial activity

The research focus on metallic NPs highlights their significant contribution to nanomedicine against Leishmania. Notably, green synthesis of metal-based NPs has shown potent antileishmanial properties favored by the presence of surface-coated phytometabolites such as flavonoids and alkaloids. In the present study, ZnO NPs were assessed
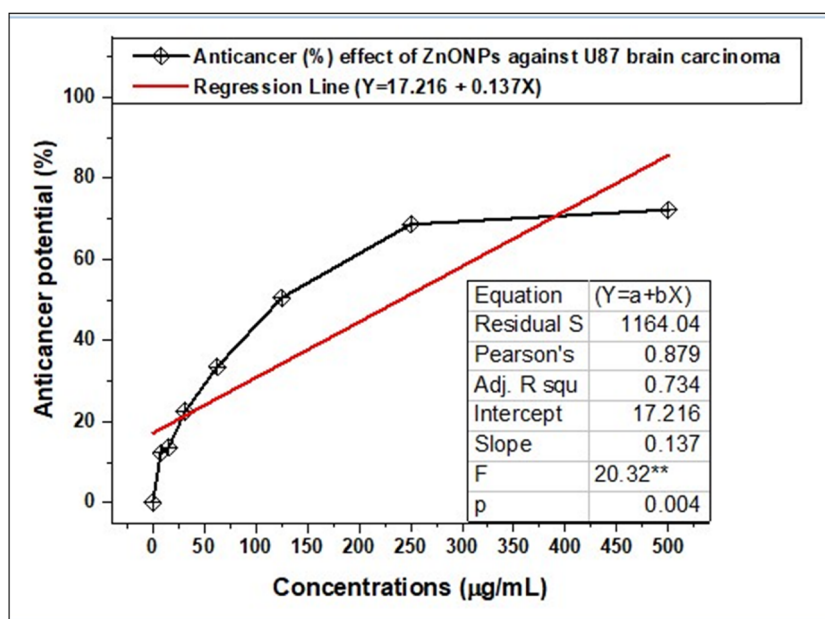

Figure 9: Least square fitting line of the cytotoxic effect of ED-ZnO NPs against U87 brain carcinoma.

Table 3: Dose-dependent responses of ED-ZnO NPs on Leishmanial cells, with an IC_{50} value

Concentration (mg·mL^{-1})	Zinc oxide nanoparticles		EC_{50} (µg·mL^{-1})	EC_{70} (µg·mL^{-1})	EC_{90} (µg·mL^{-1})	Intercept	Slope	F	R^2	p
	Mean absorbance	Percent inhibition								
20	0.167	57	20.01	21.67	29.94	17.6	2.418	5.66	0.538	0.098
15	0.177	54.4								
10	0.194	50.0								
5	0.204	47.5								
Negative control	0.388	0								

against *L. tropica* and gave convincing yielding compelling results as shown in Table 3. The results emphasize the concentration-dependent cytotoxicity, with ED-ZnO NPs significantly limiting the growth of *L. tropica*. At various doses-20, 15, 10, and 5 mg·mL^{-1} percent inhibition rates of 57%, 54.4%, 50%, and 47.5%, respectively, were observed along with corresponding IC_{50} values of 20.01 µg·mL^{-1}. These results demonstrate the pronounced lethal effect of ED-ZnO NPs against *L. tropica* and indicate the potential utility of these particles for the targeted delivery of drugs for the treatment of leishmaniasis in the nanopharmaceutical sector (Figure 10). These results are consistent with the findings of other researchers as shown in the studies conducted by Abbasi et al. [31].

3.2.10 Antihyperlipidemic and hepatoprotective activity

The results of the ED-ZnO NPs as antihyperlipidic agents are presented in Figure 11 and demonstrate a significant
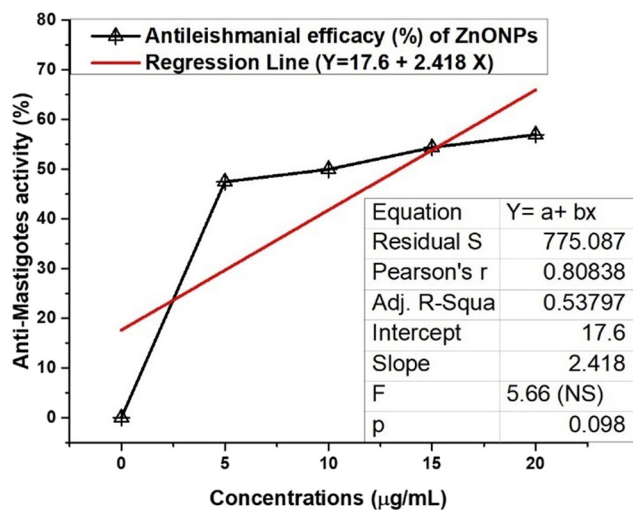
Figure 10: Least square fitting line of the anti-leishmanial effect of ED-ZnO NPs against promastigotes of *L. tropica*.

effect on cholesterol, triglyceride, LDL, and HDL levels compared to the control groups. The study documents that the group subjected to high-fat diet (consisting of vanaspati ghee and coconut oil) experienced an initial increase in cholesterol (223.5 ± 20.14), triglycerides (243.2 ± 25.22), and LDL (96.6 ± 4.56) levels, accompanied by a significant decrease in HDL (36.5 ± 11.82) levels compared to the normal diet group.

The group treated with rosuvastatin and a high-fat diet exhibited a highly significant reduction ($p < 0.01$) in cholesterol (81 ± 3.56), triglycerides (122 ± 13.18), and LDL (79 ± 6.38) and a significant increase ($p < 0.05$) in HDL compared to the high-fat diet group. The group treated with 100 mg·kg^{-1} ED-ZnO NPs and a high-fat diet showed a significant decrease in cholesterol (146.16 ± 11.0) and triglycerides (183 ± 18.75) and a non-significant increase in HDL compared to the hyperlipidemic control group. At 200 and 300 mg·kg^{-1} ED-ZnO NPs, there was a highly significant reduction in cholesterol (139.5 ± 8.82, 137.5 ± 1.81), triglycerides (139.5 ± 12.87, 131.25 ± 4.3), and LDL (36.75 ± 7.58), accompanied by a significant increase in HDL, particularly in the group treated with 300 mg·kg^{-1} ED-ZnO NPs (Figure 10). Table 3 and Figure 12 show the hepatic profile of the control group and the treated group. In this aspect, the 100 and 300 mg·kg^{-1} ED-ZnO NP-treated groups exhibited significant decreases in ALP (alkaline phosphatase), ALT, and AST. The 200 mg·kg^{-1} dose showed a significant decrease ($p < 0.05$) in ALP (101.5 ± 11.57) and a significant decrease in ALT (67.25 ± 14.19) and AST (178.0 ± 11.67) compared to the hyperlipidemia group and the rosuvastatin group. Total bilirubin levels showed no significant changes in the treated groups compared to the normal, hyperlipidemic, and rosuvastatin groups. CRI-I and CRI-II levels reached a maximum in the blood of mice fed a high diet (6.12 and 2.64, respectively), while these levels decreased these values significantly (2.08 and 0.55) when ED-ZnO NPs were administered at a dose of 300 mg·kg^{-1} body weight. The AIP and AC values significantly decline (0.29 and 1.08, respectively) with the oral administration of ED-ZnO NPs at a dose of 300 mg·kg^{-1} compared to the control (Figure 13). Overall, the study suggests
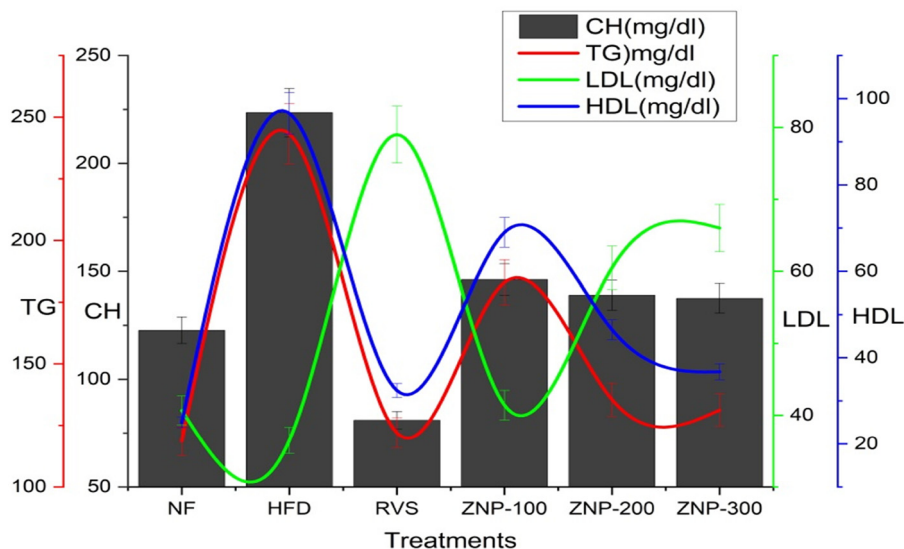
Figure 11: Effect of ED-ZnO NPs on CH, TG, LDL, and HDL profile.

that ED-ZnO NPs from *E. dracunculoides* have notable antihyperlipidemic effects and improve blood lipid profiles, hepatic markers, and renal parameters in mice hyperlipidemia-induced by hyperlipidemia.

FBS was elevated in the hyperlipidemic group compared to the normal group. The group treated with rosuvastatin demonstrated a decrease in FBS compared to the high-fat diet group. The groups treated with ZnO NPs displayed a highly significant decrease in FBS at doses of 100, 200, and 300 mg·kg^{-1} (107.2 ± 11.97, 135.0 ± 9.97, 105.25 ± 5.26, respectively) compared to the hyperlipidemic group. Creatinine and urea levels also decreased significantly (33.75 and 0.48 mg·dL^{-1}) in the groups treated with ED-ZnO NPs (Figure 14). Overall,

these results suggest that ZnO NPs effectively reduced hyperlipidemia, helped restore hepatic enzyme levels, and played a role in regulating creatinine and blood glucose levels. This highlights the potential of ZnO NPs as effective antihyperlipidemic agents capable of mitigating hyperlipidemia-associated complications and restoring renal function.

4 Discussion

Metallic NPs, particularly ED-ZnO NPs, have recently gained attention due to their extensive physiochemical properties.
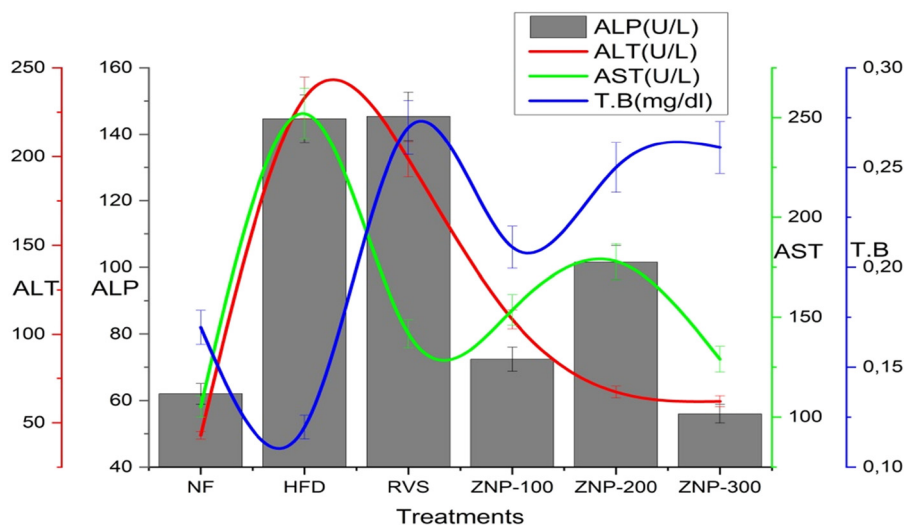

Figure 12: Effect of ED-ZnO NPs on ALP, AST, ALT, and total serum bilirubin.
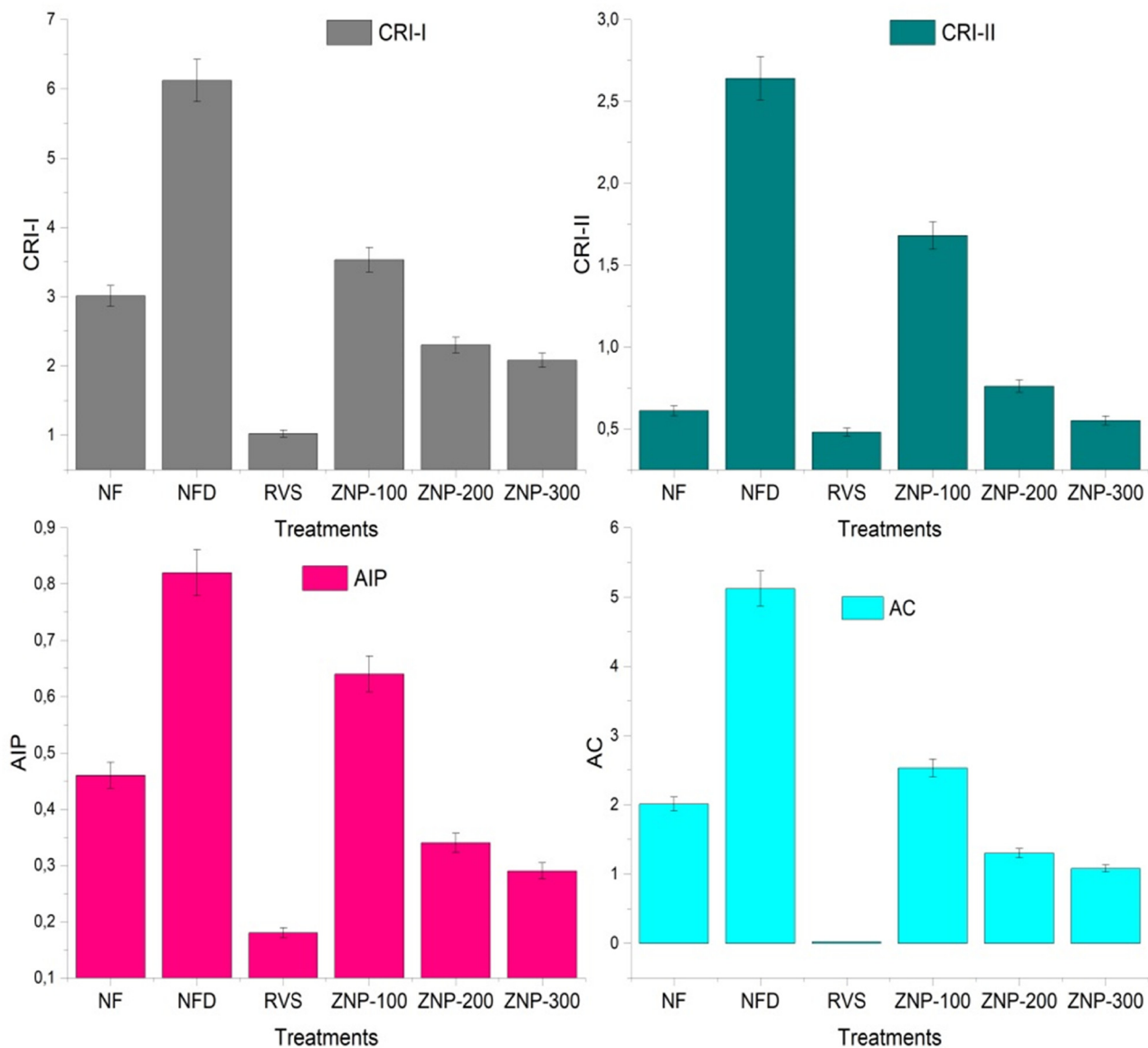
Figure 13: Effect of ED-ZnO NPs on CRI-I, CRI-II, AIP, and AC.

In the present study, we synthesized ED-ZnO NPs using the methanol extract of *E. dracunculoides* as a reducing agent and then evaluated their biological potential. Prior to the *in vivo* and *in vitro* drug release study, the biologically produced ED-ZnO NPs were characterized by various techniques, e.g., UV spectroscopy. FTIR analysis shows several variations in the ED-ZnO NPs spectrum indicating different functional groups showing stabilization of pharmaceutically potent bioactive compounds, which was confirmed by GC–MS analysis with Zn in ED-ZnO NPs. The FTIR spectrum results are confirmed by SEM, TEM, XRD, and EDX analyses of the NPs. The XRD analysis helped in the identification of NPs using Scherrer's equation. The results suggest a size of 70–95 nm with a crystalline nature. Our results are in agreement with the findings of Yang et al. [32]. SEM analysis was performed to determine the morphological state of the ED-ZnO NPs. This analysis shows that the NPs are mostly spherical and irregular in shape. The purity of the ED-ZnO NPs was confirmed by EDX analysis, which indicated the presence of the element Zn and other organic compounds, i.e. O and C, suggesting the presence of biologically active compounds, as the extract of *E. dracunculoides* contains various organic compounds consisting of O, H, and C.

The mortality and morbidity rates due to cancer are increasing day by day worldwide. Currently, about 19.9 million cases have been reported and the number is
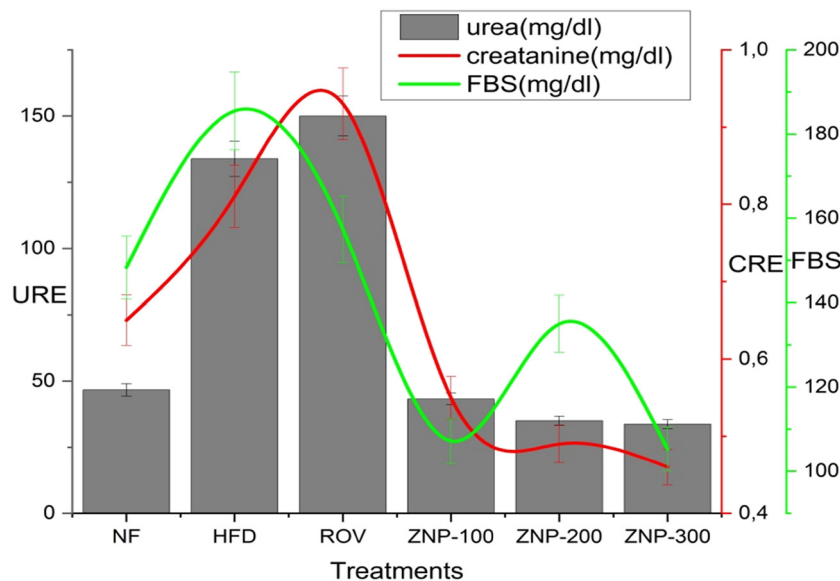
Figure 14: Effect of ED-ZnO NPs on blood urea, creatinine, and fasting blood sugar.

expected to rise to 28.4 million in the next 20 years. Various techniques have been used to reduce the prevalence rate of cancer, but unfortunately, no one has succeeded in this field to eradicate this prevalent disease. In the present times, researchers are trying their best to save the people of the world from this dangerous disease by adopting a green nano-approach. There is an abundance of research data reporting the antitumor potential of NPs. Recently, Haq et al. [33] reported the significant anticancer potential of S-CeONPs against various cell lines. In our current study, the ED-ZnO NPs show promising antitumor activity against U87 brain cells. The tumor cell toxicity of ED-ZnO NPs may be attributed to their unique band gap and catalytic activity [34,35]. ZnO NPs have also been reported to increase that ZnO NPs enhance the production of ROS and induce oxidative stress, ultimately leading to an increased rate of apoptosis and subsequent cancer cell death [36–39]. Furthermore, a number of studies have reported deleterious cellular effects of ZnO NPs in different cell systems, including genetic damage, alterations in cell organelle functions and structure, cell cycle disruption, cell death induction, and cell membrane impairment [40,41]. This multifaceted approach highlights the potential of ED-ZnO NPs in improving cancer therapy outcomes through their ability to induce apoptosis via ROS production and oxidative stress. Importantly, the results of this study demonstrate that ED-ZnO NPs exhibit selective cytotoxicity in a dose- and time-dependent manner against cancer cells while having no obvious impact on non-malignant cells. The cytotoxic effect of the NPs could be due to diverse phytochemicals present in the methanol extract of the test plant that encapsulates the metallic Zn. Little is known about the possible effects or

mechanism of action of ZnO NPs on cells of the nervous system. These results demonstrate the potential of ED-ZnO NPs as an effective anti-cancer. In particular, these observations are consistent with previous studies by Lingaraju et al. [42]. Another recent study demonstrated a similar effect on viability (MTT assay) in a primary culture of rat astrocytes, finding a decrease in cell viability as a function of dose and exposure time, with cytotoxic effects starting at $30\,\mu g\cdot mL^{-1}$ after 24 h of ZnO NP exposure [43]. Sharma et al. also found a dose-dependent increase in cell death in mouse N9 microglia after 24 h of treatment with ZnO NPs (>50 nm, $1–100\,\mu g\cdot mL^{-1}$) [44]. In this case, however, a more extreme cytotoxic effect was observed than in astrocytes, which is reflected in the lower IC_{50} value ($6.612\,\mu g\cdot mL^{-1}$ ZnO NP).

Leishmaniasis is an infectious disease caused by the protozoan parasite Leishmania, a member of the *Trypanosomatid* genus [45]. The commercially available treatments for leishmaniasis are characterized by their high cost, toxicity, and limited efficacy. However, various alkaloids belonging to different classes and a number of flavonoids derived from plants have shown potent antileishmanial activities. These compounds act by inhibiting topoisomerase II in the Leishmania parasite, thereby disrupting the cell cycle and exerting their efficacy [46]. Linalool terpenoids, another class of compounds, exhibit a vigorous ability to induce the formation of nitric oxide radicals in the macrophages of infected cells. These terpenoids are associated with significant alterations in mitochondria, kinetoplasts, and nuclear chromatins, which contributes to their antileishmanial effects [47]. The multifaceted mechanisms of action of these natural products emphasize their potential in the control of leishmaniasis and offer

promising opportunities for the development of novel therapeutic strategies. Various metal oxides have been tested *in vitro* for their cytotoxicity in the control of Leishmania situations [48]. Metallic NPs have been shown to impede the growth of Leishmania through various mechanisms, including inhibition of enzymes, membrane damage, and induction of apoptosis via the generation of ROS [49,50]. These NPs stimulate the intracellular production of ROS and thereby cause damage to DNA, oxidize lipids and proteins, and ultimately lead to cell death [51].

Hyperlipidemia has long been recognized as a contributing factor to the progression of atherosclerosis and cardiovascular disease [52]. In the context of lipid transport, LDL-C is a primary carrier of TC. Elevated LDL-C levels can lead to an accumulation of cholesterol in the blood vessel walls, which directly promotes the development of atherosclerotic plaques [53]. In contrast, HDL plays a protective role, as it facilitates the transfer of cholesterol from peripheral tissues to the liver via "reverse cholesterol transport" and thus contributes to its degradation. Higher triglyceride and LDL levels are also associated with been linked to coronary heart disease [54].

The results of ZnO NPs (ED-ZnO NPs) derived from *E. dracunculoide*s show beneficial effects on blood lipid profiles in mice by improving lipid metabolism disorders induced by resulting from high-fat emulsions and also significantly restoring the levels of liver enzymes such as ALT, AST, ALP, and total bilirubin. The antihyperlipidemic and hepatoprotective effects of the NPs can be attributed to their chemical composition, which includes phytochemicals such as flavonoids, saponins, cardiac glycosides, and alkaloids that have been shown to reduce serum lipid levels in animal models [55]. In summary, this study highlights the potential of ED-ZnO NPs from *E. dracunculoide*s to effectively counter hyperlipidemia. The antihyperlipidemic effects are thought to be mediated by the chemical constituents of the NPs, which is consistent with previous studies that have demonstrated their lipid-lowering properties. This suggests a promising avenue for the use of NPs in the treatment of hyperlipidemia and its associated health risks. The study encompassed an examination of changes associated with hypercholesterolemia, specifically increased hepatic inflammatory markers, FBS, and changes in renal profile changes. The remarkable reduction of cholesterol, triglycerides, and LDL in all treated groups could be attributed to the presence of flavonoids and phytosterols in *E. dracunculoide*s. Furthermore, studies have indicated that compounds such as *cis* octadecanoic acid and octadecanoic acid (stearic acid) have a hypolipidemic effect [56]. Other compounds, such as botulin, ß-sitosterol, and ergost-8(14)-en-3-ol, have been reported to have hepatoprotective and antihyperlipidemic effects as well as various other biological

potentials [57] but our results show a significant difference among the biological potential of ED-ZnO NPs and the methanol extract of *E. dracunculoide*s used alone. The superiority of the biological potential of ED-ZnO NPs may be due to the unique physiochemical properties and nanostructure, which further boost the biological potential of the active phytochemicals from the plant involved in processes such as reduction, capping, and stabilization of Zn oxide.

5 Conclusion

The biosynthesized ZnO NPs showed remarkable activities in various medical applications. The NPs showed efficacy against cancer (mortality rate 72.25%) and against leishmaniasis (inhibition rate 57%), suggesting a promising effect in combating these diseases. Moreover, their antihyperlipidemic properties have been demonstrated by their ability to regulate blood lipid profiles and mitigate the complications associated with hyperlipidemia ED-ZnO NPs also restore the levels of ALP (101.5 U·L^{-1}), ALT (67.25 U·L^{-1}), AST (178 U·L^{-1}), total bilirubin (0.26 mg·dL^{-1}), creatinine (33.75 mg·dL^{-1}), urea (0.48 mg·dL^{-1}), and glucose (105.25 mg·dL^{-1}) compared to the control. The comprehensive results indicate that ZnO NPs have significant potential for various medical purposes in all modalities. However, further research on ZnO NPs is required to fully exploit their biological capabilities both *in vitro* and *in vivo*. This work can be useful for pharmacologists to find safe and cost-effective drugs instead of synthetic drugs to cure various ailments.

Author contributions: Conceptualization: UK, SJ, RU, and MNK. Data curation: RU, MNK, UK, RU, and MAA. Writing – original draft: UK and TuH. Formal analysis: MAA, MFE, MNK, and MI. Investigation: TuH, UK, and MNK. Methodology: MAA, AR, UK, and RU. Validation: MFE, UK, and SJ. Visualization and resources: MAA, AR, AK, and MI. Writing – review and editing; AR, AK, and MFE. All authors contributed significantly and have read and agreed to the published version of the article.

Conflict of interest: Authors state no conflict of interest.

Data availability statement: All data generated or analyzed during this study are included in this published article.

References

[1] GnanaJobitha G, Annadurai G, Kannan C. Green synthesis of silver nanoparticle using *Elettaria cardamomom* and assesment of its antimicrobial activity. Int J Pharma Sci Res (IJPSR). 2012;3:323–30.

[2] Zafar MN, Dar Q, Nawaz F, Zafar MN, Iqbal M, Nazar MF. Effective adsorptive removal of azo dyes over spherical ZnO nanoparticles. J Mat Res Technol. 2019;8:713–25. doi: 10.1016/j.jmrt.2018. 06.002.

[3] Vasantharaj S, Sathiyavimal S, Senthilkumar P, LewisOscar F, Pugazhendhi A. Biosynthesis of iron oxide nanoparticles using leaf extract of *Ruellia tuberosa*: antimicrobial properties and their applications in photocatalytic degradation. J Photochem Photobiol B. 2019;192:74–82. doi: 10.1016/j. jphotobiol.2018.12.025.

[4] Mazur M. Electrochemically prepared silver nanoflakes and nano-wires. Electrochem Commun. 2004;6:400–3. doi: 10.1016/j.elecom. 2004.02.011.

[5] Hailu YM, Atlabachew M, Chandravanshi BS, Redi-Abshiro M. Composition of essential oil and antioxidant activity of Khat (*Catha edulis* Forsk), Ethiopia. Chem Int. 2017;3:25–31.

[6] Dagnaw W, Mekonnen A. Preliminary phytochemical screening, isolation and structural elucidation of chloroform leaf extracts of *Maesa lanceolata*. Chem Int. 2017;3:351–7.

[7] Benouis K. Phytochemicals and bioactive compounds of pulses and their impact on health. Chem Int. 2017;3:224–9.

[8] Cahyana AH, Kam N, Ellyn. Study on the stability of antioxidant and anti-glucosidase activities using soaking treatment of Okra (*Abelmoschus esculentus* L.) mucilage extracts. Chem Int. 2017;3:203–12.

[9] Zinatloo-Ajabshir S, Morassaei MS, Salavati-Niasari M. Facile fabrication of Dy2 Sn_2O_7-SnO_2 nanocomposites as an effective photocatalyst for degradation and removal of organic contaminants. J Colloid and Interface Sci. 2017;497:298–308. doi: 10.1016/j.jcis.2017.03.031.

[10] Salavati-Niasari M, Mohandes F, Davar F. Preparation of PbO nanocrystals via decomposition of lead oxalate. Polyhedron. 2009;28:2263–7. doi: 10.1016/j.poly.2009.04.009.

[11] Mishra PK, Mishra H, Ekielski A, Talegaonkar S, Vaidya B. Zinc oxide nanoparticles: a promising nanomaterial for biomedical applications. Drug Discovery Today. 2017;22:1825–34. doi: 10 .1016/j. drudis.2017.08.006.

[12] Arvanag FM, Bayrami A, Habibi-Yangjeh A, Pouran SR. A comprehensive study on antidiabetic and antibacterial activities of ZnO nanoparticles biosynthesized using *Silybum marianum* L seed extract. Mater Sci Eng: C. 2019;97:397–405. doi: 10.1016/j.msec. 2018.12.058.

[13] Jamdagni P, Khatri P, Rana JS. Green synthesis of zinc oxide nanoparticles using flower extract of *Nyctanthes arbor-tristis* and their antifungal activity. J King Saud Univ Sci. 2018;30:168–75. doi: 10.1016/j.jksus.2016.10.002.

[14] Umar H, Kavaz D, Rizaner N. Biosynthesis of zinc oxide nanoparticles using *Albizia lebbeck* stem bark, and evaluation of its antimicrobial, antioxidant, and cytotoxic activities on human breast cancer cell lines. Int J Nanomed. 2019;20:87–100. doi: 10.2147/IJN. S186888.

[15] Dhillon GS, Kaur S, Brar SK. Facile fabrication and characterization of chitosan-based zinc oxide nanoparticles and evaluation of their antimicrobial and antibiofilm activity. Int Nano Lett. 2014;4:1–11. doi: 10.1007/s40089-014-0107-6.

[16] Parthasarathy G, Saroja M, Venkatachalam M, Evanjelene V. Biological synthesis of zinc oxide nanoparticles from leaf extract of *Curcuma neilgherrensis* wight. Int J Mat Sci. 2017;12:73–86.

[17] Wang L, Ma YT, Sun QY, Li XN, Yan Y, Yang J, et al. Structurally diversified diterpenoids from *Euphorbia dracunculoides*. Tetrahedron. 2015;71:5484–93. doi: 10.1016/j.tet.2015.06.078.

[18] Sharma J, Painuli R, Gaur R. Plants used by the rural communities of district Shahjahanpur, Uttar Pradesh. Indian J Tradit Knowl. 2010;9:798–803.

[19] Shah NA, Khan MR, Naz K, Khan MA. Antioxidant potential, DNA protection, and HPLC-DAD analysis of neglected medicinal Jurinea dolomiaea roots. BioMed Res Int. 2014;2014:726241.

[20] Vijayakumar S, Mahadevan S, Arulmozhi P, Sriram S, Praseetha P. Green synthesis of zinc oxide nanoparticles using *Atalantia monophylla* leaf extracts: Characterization and antimicrobial analysis. Mat Sci Semicond Process. 2018;82:39–45. doi: 10.1016/j.mssp.2018. 03.017.

[21] Rezadoost MH, Kumleh HH, Ghasempour A. Cytotoxicity and apoptosis induction in breast cancer, skin cancer and glioblastoma cells by plant extracts. Mol Biol Rep. 2019;46:5131–42. doi: 10.1007/ s11033-019-04970-w.

[22] Mahmoudvand H, Sharififar F, Rahmat MS, Tavakoli R, Dezaki ES, Jahanbakhsh S, et al. Evaluation of antileishmanial activity and cytotoxicity of the extracts of *Berberis vulgaris* and *Nigella sativa* against *Leishmania tropica*. J Vector Borne Dis. 2014;51:294–9.

[23] Mirzaie M, Nosratabadi SJ, Derakhshanfar A, Sharifi I. Antileishmanial activity of *eganum harmala* extract on the *in vitro* growth of *Leishmania major* promastigotes in comparison to a tri-valent antimony drug. Vet Arh. 2007;77:365–75.

[24] Khan SJ, Afroz S, Khan RA. Antihyperlipidemic and anti-hyperglycemic effects of *Cymbopogon jwarancusa* in high-fat high-sugar diet model. Pak J Pharm Sci. 2018;31:1341–5.

[25] Jayappa MD, Ramaiah CK, Kumar MAP, Suresh D, Prabhu A, Devasya RP, et al. Green synthesis of zinc oxide nanoparticles from the leaf, stem and *in vitro* grown callus of *Mussaenda frondosa* L.: characterization and their applications. Appl Nanosci. 2020;10:3057–74. doi: 10.1007/s13204-020-01382-2.

[26] Rahaiee S, Ranjbar M, Azizi H, Govahi M, Zare M. Green synthesis, characterization, and biological activities of saffron leaf extract-mediated zinc oxide nanoparticles: a sustainable approach to reuse an agricultural waste. Appl Organomet Chem. 2020;34:1–12. doi: 10.1002/aoc.5705.

[27] Fardood TS, Moradnia F, Ghalaichi AH, Danesh Pajouh S, Heidari M. Facile green synthesis and characterization of zinc oxide nanoparticles using tragacanth gel: investigation of their photocatalytic performance for dye degradation under visible light irradiation. Nanochem Res. 2020;5:69–76. doi: 10.22036/NCR.2020.01.007.

[28] Datta A, Patra C, Bharadwaj H, Kaur S, Dimri N, Khajuria R. Green synthesis of zinc oxide nanoparticles using *Parthenium hysterophorus* leaf extract and evaluation of their antibacterial properties. J Biotechnol Biomater. 2017;7:271–6. doi: 10.4172/2155-952X.1000271.

[29] Singh J, Kumar S, Alok A, Upadhyay SK, Rawat M, Tsang DC, et al. The potential of green synthesized zinc oxide nanoparticles as nutrient source for plant growth. J Clean Prod. 2019;214:1061–70. doi: 10.1016/j.jclepro.2019.01.018.

[30] Vinayagam R, Selvaraj R, Arivalagan P, Varadavenkatesan T. Synthesis, characterization and photocatalytic dye degradation capability of *Calliandra haematocephala*-mediated zinc oxide nanoflowers. J Photochem Photobiol B. 2020;203:1–9. doi: 10.1016/j. jphotobiol.2019.111760.

[31] Abbasi BH, Anjum S, Hano C. Differential effects of *in vitro* cultures of *Linum usitatissimum* L. (Flax) on biosynthesis, stability, antibacterial and antileishmanial activities of zinc oxide nanoparticles: A

mechanistic approach. RSC Adv. 2017;7:15931–43. doi: 10.1039/c7ra02070h.

[32] Yang KY, Hwang DH, Yousaf AM, Kim DW, Shin YJ, Bae ON, et al. Silymarin-loaded solid nanoparticles provide excellent hepatic protection: physicochemical characterization and *in vivo* evaluation. Int J Nanomed. 2013;8:3333–43. doi: 10.2147/IJN.S50683.

[33] Haq T, Ullah R, Khan MN, Wahab S, Ali B, Kaplan A, et al. Phyto-drug (silymarin)-encapsulated cerium oxide nanoparticles (S-CeONPs) for *In-vitro* release, ameliorating antimicrobial, anticancer, anti-inflammatory and antioxidant potential. BioNanoScience. 2024;1–15. doi: 10.1007/s12668-023-01295-8.

[34] Punnoose A, Dodge K, Rasmussen JW, Chess J, Wingett D, Anders C. Cytotoxicity of ZnO nanoparticles can be tailored by modifying their surface structure: A green chemistry approach for safer nanomaterials. ACS Sustainable Chem Eng. 2014;2:1666–73. doi: 10.1021/sc500140x.

[35] Sindhura KS, Prasad T, Selvam PP, Hussain O. Synthesis, characterization and evaluation of effect of phytogenic zinc nanoparticles on soil exo-enzymes. Appl Nanosci. 2014;4:819–27. doi: 10.1007/s13204-013-0263-4.

[36] Kim SH, Yook TH, Kim JU. Rehmanniae radix, an effective treatment for patients with various inflammatory and metabolic diseases: Results from a review of Korean publications. J Pharmacopuncture. 2017;20:81–8. doi: 10.3831/KPI.2017.20.010.

[37] Vaez Z, Javanbakht V. Synthesis, characterization and photocatalytic activity of ZSM-5/ZnO nanocomposite modified by Ag nanoparticles for methyl orange degradation. J Photochem Photobiol A. 2020;388:1–11. doi: 10.1016/j.jphotochem.2019.112064.

[38] Abdelsattar AS, Makky S, Nofal R, Hebishy M, Agwa MM, Aly RG, et al. Enhancement of wound healing via topical application of natural products: *in vitro* and *in vivo* evaluations. Arab J Chem. 2022;15:1–20. doi: 10.1016/j.arabjc.2022.103869.

[39] Bhat MP, Kumar RS, Almansour AI, Arumugam N, Dupadahalli K, Rudrappa M, et al. Characterization, antimicrobial activity and anticancer activity of *Pyrostegia venusta* leaf extract-synthesized silver nanoparticles against COS-7 cell line. Appl Nanosci. 2023;13:2303–14. doi: 10.1007/s13204-021-02120-y.

[40] Singh S. Zinc oxide nanoparticles impacts: cytotoxicity, genotoxicity, developmental toxicity, and neurotoxicity. Toxicol Mech Methods. 2019;29:300–11.

[41] Demir E. A review on nanotoxicity and nanogenotoxicity of different shapes of nanomaterials. J Appl Toxicol. 2021;41:118–47.

[42] Lingaraju K, Naika HR, Nagabhushana H, Nagaraju G. *Euphorbia heterophylla* (L.) mediated fabrication of ZnO NPs: Characterization and evaluation of antibacterial and anticancer properties. Biocatal Agric Biotechnol. 2019;18:1–8. doi: 10.1016/j.bcab.2018.10.011.

[43] Sudhakaran S, Athira SS, Mohanan PV. Zinc oxide nanoparticle induced neurotoxic potential upon interaction with primary astrocytes. Neurotoxicology. 2019;73:213–27.

[44] Sharma AK, Singh V, Gera R, Purohit MP, Ghosh D. Zinc oxide nanoparticle induces microglial death by NADPHOxidase-inde-pendent reactive oxygen species as well as energy depletion. Mol Neurobiol. 2017;54:6273–86.

[45] Singh N, Kumar M, Singh RK. Leishmaniasis: current status of available drugs and new potential drug targets. Asian Pac J Trop Med. 2012;5:485–97. doi: 10.1016/S1995-7645(12)60084-4.

[46] Aissani N, Albouchi F, Sebai H. Anticancer effect in human glioblastoma and antioxidant activity of *Petroselinum crispum* L. methanol extract. Nutr Cancer. 2021;73:2605–13. doi: 10.1080/01635581.2020.1842894.

[47] Newman DJ, Cragg GM. Natural products as sources of new drugs from 1981 to 2014. J Nat Prod. 2016;79:629–61. doi: 10.1021/acs.jnatprod.5b01055.

[48] de Souza PO, Bianchi SE, Figueiró F, Heimfarth L, Moresco KS, Gonçalves RM, et al. Anticancer activity of flavonoids isolated from *Achyrocline satureioides* in gliomas cell lines. Toxicol in vitro. 2018;51:23–33. doi: 10.1016/j.tiv.2018.04.013.

[49] Darwish AGG, Samy MN, Sugimoto S, Matsunami K, Otsuka H. *In vitro* antileishmanial activity of methanolic extracts for some selected medicinal plants. Pharmacogn Mag. 2019;15:34–7. doi: 10.4103/pm.pm_570_18.

[50] Et-Touys A, Fellah H, Sebti F, Mniouil M, Aneb M, Elboury H, et al. *In vitro* antileishmanial activity of extracts from endemic Moroccan medicinal plant S*alvia verbenaca* (L.) Briq. ssp *verbenaca* Maire (S. *clandestina* Batt. non L). Eur J Med Plants. 2016;16:1–8. doi: 10.9734/EJMP/2016/27891.

[51] Camacho MDR, Phillipson JD, Croft SL, Rock P, Marshall SJ, Schiff PL. *In vitro* activity of *Triclisia paten*s and some bisbenzylisoquinoline alkaloids against eishmania donovani and *Trypanosoma brucei brucei*. Phytother Res. 2002;16:432–6. doi: 10.1002/ptr.929.

[52] Szidonya L, Hunyady L. A transgenic model of visceral obesity and the metabolic syndrome. Trends Endocrinol Metab. 2002;13:98. doi: 10.1016/S1043-2760(02)00581-7.

[53] Zhu J, Liu W, Yu J, Zou S, Wang J, Yao W, et al. Characterization and hypoglycemic effect of a polysaccharide extracted from the fruit of *Lycium barbarum* L. Carbohydr Polym. 2013;98:8–16. doi: 10.1016/j.carbpol.2013.04.057.

[54] Chang JJ, Chen TH, Chan P, Chen YJ, Hsu FL, Lo MY, et al. The *in vitro* inhibitory effect of tannin derivatives on 3-hydroxy-3-methylglutaryl-coenzyme A reductase on vero cells. Pharmacology. 2001;62:224–8. doi: 10.1159/000056099.

[55] Abdel-Hassan IA, Abdel-Barry JA, Mohammeda ST. The hypoglycaemic and antihyperglycaemic effect of *Citrullu*s *colocynthi*s fruit aqueous extract in normal and alloxan diabetic rabbits. J Ethnopharmacol. 2000;71:325–30. doi: 10.1016/s0378-8741(99)00215-9.

[56] Igwe K, Nwankwo P, Otuokere I, Ijioma S, Amaku F. GC-MS analysis of phytocomponents in the methanolic extract of *Moringa oleifera* leave. J Res Pharm Sci. 2015;2:1–6.

[57] Rajasekaran S, Sivagnanam K, Ravi K, Subramanian S. Hypoglycemic effect of *Aloe vera* gel on streptozotocin-induced diabetes in experimental rats. J Med Food. 2004;7:61–6. doi: 10.1089/109662004322984725.